

Cubic anisotropy in (Ga,Mn)As layers: Experiment and theory

M. Sawicki, O. Proselkov, C. Sliwa, P. Aleshkevych, and J. Z. Domagala

Institute of Physics, Polish Academy of Sciences, Aleja Lotnikow 32/46, PL-02668 Warsaw, Poland

J. Sadowski

*Institute of Physics, Polish Academy of Sciences, Aleja Lotnikow 32/46, PL-02668 Warsaw, Poland;**MAX-IV laboratory, Lund University, P.O. Box 118, SE-22100 Lund, Sweden;**and Department of Physics and Electrical Engineering, Linnaeus University, SE-391 82 Kalmar, Sweden*

T. Dietl

*International Research Centre MagTop, Aleja Lotnikow 32/46, PL-02668 Warsaw, Poland;**Institute of Physics, Polish Academy of Sciences, Aleja Lotnikow 32/46, PL-02668 Warsaw, Poland;**and WPI-Advanced Institute for Materials Research, Tohoku University, Sendai 980-8577, Japan*

(Received 31 January 2018; published 3 May 2018)

Historically, comprehensive studies of dilute ferromagnetic semiconductors, e.g., p -type (Cd,Mn)Te and (Ga,Mn)As, paved the way for a quantitative theoretical description of effects associated with spin-orbit interactions in solids, such as crystalline magnetic anisotropy. In particular, the theory was successful in explaining *uniaxial* magnetic anisotropies associated with biaxial strain and nonrandom formation of magnetic dimers in epitaxial (Ga,Mn)As layers. However, the situation appears much less settled in the case of the *cubic* term: the theory predicts switchings of the easy axis between in-plane $\langle 100 \rangle$ and $\langle 110 \rangle$ directions as a function of the hole concentration, whereas only the $\langle 100 \rangle$ orientation has been found experimentally. Here, we report on the observation of such switchings by magnetization and ferromagnetic resonance studies on a series of high-crystalline quality (Ga,Mn)As films. We describe our findings by the mean-field p - d Zener model augmented with three new ingredients. The first one is a scattering broadening of the hole density of states, which reduces significantly the amplitude of the alternating carrier-induced contribution. This opens the way for the two other ingredients, namely the so-far disregarded single-ion magnetic anisotropy and disorder-driven nonuniformities of the carrier density, both favoring the $\langle 100 \rangle$ direction of the apparent easy axis. However, according to our results, when the disorder gets reduced, a switching to the $\langle 110 \rangle$ orientation is possible in a certain temperature and hole concentration range.

DOI: [10.1103/PhysRevB.97.184403](https://doi.org/10.1103/PhysRevB.97.184403)**I. INTRODUCTION**

The discovery of carrier-mediated ferromagnetism in (III,Mn)V and (II,Mn)VI semiconductor systems makes it possible to examine the interplay between the physical properties of semiconductor quantum structures and ferromagnetic materials [1]. At the same time, complementary resources of these systems allowed for novel functionalities and devices enabling magnetization manipulation [1–5], paving the way towards the industrial development stage for all-metal devices [5,6]. In this context (Ga,Mn)As has served as a valuable test ground for new concepts and device architecture, due to the relatively high Curie temperature T_C and its compatibility with the well-characterized GaAs system. Importantly, despite much lower spin and carrier concentrations compared to ferromagnetic metals, (III,Mn)V dilute ferromagnetic semiconductors (DFS) exhibit excellent micromagnetic characteristics, including well defined magnetic anisotropy and large ferromagnetic domains. The theoretical understanding of these materials is built on the p - d Zener model of ferromagnetism [7]. In this model, the thermodynamic properties are determined by the valence-band carriers contribution to the free energy of the system, which is

calculated taking the spin-orbit interaction into account within the $\mathbf{k} \cdot \mathbf{p}$ theory [7–11] or tight-binding model [12,13] with the p - d exchange interaction between the carriers and the localized Mn spins considered within the virtual-crystal and molecular-field approximations. In this approach, the long-range ferromagnetic interactions between the localized spins are mediated by delocalized holes in the weakly perturbed p -like valence band [14].

The model explains well the influence of epitaxial strain on magnetic anisotropy and various experimentally observed magnetic easy axis spin reorientation transitions (SRT) as a function of temperature T and hole concentration p with a sound exception of the fourfold (cubiclike) component of the magnetic anisotropy for which neither a strong oscillatory dependence $\langle 100 \rangle \leftrightarrow \langle 110 \rangle$ on p and T (through magnetization M) nor its predicted strength have been verified [10,11,15–18]. Intriguingly, only the $\langle 100 \rangle$ in-plane cubic easy axis directions have been reported in (Ga,Mn)As epilayers so far [18–25].

In this study, we provide experimental evidence that the $\langle 110 \rangle$ in-plane directions can become the cubic easy axes in (Ga,Mn)As. These observations stem from the examination of magnetization curves and angular dependencies of the

ferromagnetic resonance (FMR) of carefully selected and prepared thin (Ga,Mn)As layers. Interestingly, the $\langle 110 \rangle$ cubic easy axes are observed only in limited ranges of p and T , indicating an oscillating nature ($\langle 100 \rangle \leftrightarrow \langle 110 \rangle$ easy axis switching) of the cubic anisotropy as a function of T and/or p .

The effect elaborated here is of a significant supportive value for the p - d Zener approach to ferromagnetism of DFS in general and for the (III,Mn)V family in particular. It confirms perhaps the last experimentally unproven qualitative prediction of the model: the oscillatory behavior of the cubic easy axis [8]. On the other hand, we show that our experimental findings are richer than the model can describe, even in the advanced form developed here to incorporate contributions from the single-ion anisotropy of $S = 5/2$ Mn spin and the disorder. So, to reconcile the *experimental* findings with the model computations, we include semiquantitatively into our data analysis the well established, but somehow largely disregarded fact that the assumption of an excellent magnetic homogeneity of very thin (Ga,Mn)As layers is not valid due to two space-charge layers, which are formed at the material interfaces [26–29]. These interfacial charges deplete considerably the two near-the-interface regions of (Ga,Mn)As, introducing a certain amount of electrical disorder into even the best optimized samples. Then, on the account of the increasing magnitude of the fluctuations in the local hole density of states [30,31], the long-range ferromagnetic (FM) coupling expected in an ideal high- p and an edgeless material, acquires in these regions a mesoscopic character and superparamagnetic-like (SP-L) properties are added to the expected “ideal” magnetic response of the bulk (Ga,Mn)As films [32]. Basing on some heuristic experimental considerations, our study convincingly shows that this is the presence of this SP-L response, whose magnetic characteristics greatly resemble the $\langle 100 \rangle$ -easy axis cubic anisotropy behavior, that is most likely responsible for an apparent rotation of the cubic anisotropy to $\langle 100 \rangle$ direction at low T and/or low p in our samples. In this context, our study appears to be a sizable step to bridge the gap that has separated the experiment and the theory in this field.

II. SAMPLES AND EXPERIMENT

A range of $10 < d < 20$ -nm-thin (Ga,Mn)As layers with Mn composition $x \simeq 10\%$ has been deposited with a use of arsenic valve cracker effusion cell at 190°C by LT molecular beam epitaxy on about 18×20 -mm² GaAs (100) substrates buffered with 20-nm-thick LT-GaAs. One of the layers have been subjected to *in situ* LT annealing under As capping [33], whereas the rest of the layers are investigated in their as grown state or are subject to conventional open air oven LT annealing [34] at 180°C . Their high structural quality has been confirmed by x-ray diffraction using laboratory Philips x-ray high-resolution X’Pert MRD diffractometer with samples mounted on a high precision goniometric stage. Figure 1 demonstrates $2\theta/\omega$ curves for the 004 Bragg reflection for samples from this study. As typically for (Ga,Mn)As deposited on GaAs substrates, the layers are fully strained, i.e., they have the same in-plane lattice parameter as that of the substrate. Diffraction peaks corresponding to the (Ga,Mn)As epitaxial layers shift to smaller angles with respect to that of the GaAs substrate, as a result of larger perpendicular lattice parameters. Clear

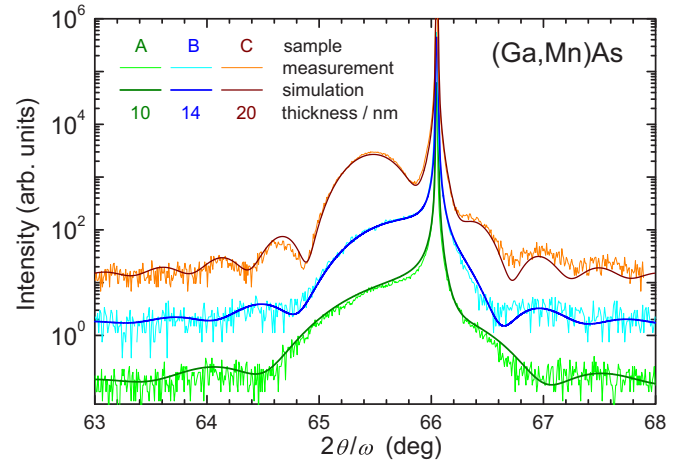


FIG. 1. Fine lines of lighter shades mark high-resolution x-ray diffraction patterns of the studied (Ga,Mn)As layers: 004 Bragg reflection, $2\theta/\omega$ scans. The central narrow features represent reflections from the GaAs substrate and the broader peaks at lower angles are reflections from the layers. Thicker lines of darker shades mark simulations upon which Mn concentrations and the layers thicknesses have been established. Curves are shifted vertically to increase clarity of the presentation.

x-ray interference fringes imply a high structural perfection of the layers and good quality of the interfaces. Mn content and layer thickness d are established upon simulation (marked as thicker solid lines of darker shades in Fig. 1) performed using commercially available PANALYTICAL EPITAXY software based on the dynamical theory of x-ray diffraction assuming elastic stiffness constants as for bulk GaAs and linear dependence of the lattice parameter of (Ga,Mn)As on x : $a(x) = 5.65469 + 0.24661x$ [35]. The results are listed in Table I.

Layers presented in this study have been selected according to their best lateral homogeneity, which has been assessed by T_C mapping across the substrate. We note that whereas T_C variations approaching up to 40% in ferromagnetic (Ga,Mn)N [36] and exceeding 5% in (Ga,Mn)As are typically observed across similar substrates, in the three layers reported here, as indicated in Table I, the spread of their T_C values across the whole 2-cm substrate is smaller than 2 K, i.e., below 2%. Importantly, only in such layers cubic easy axes are found to be oriented along $\langle 110 \rangle$.

Magnetic measurements are carried out in a commercial MPMS XL Superconducting Quantum Interference Device (SQUID) magnetometer equipped with a low field option. Customary cut long Si strips are facilitating samples support

TABLE I. List of the (Ga,Mn)As layers investigated in this study for which the easy axes of the cubic magnetic anisotropy have been found to be aligned along $\langle 110 \rangle$ in-plane orientations. Mn content and thickness are determined upon x-ray diffraction pattern modeling.

| Sample | Mn content % | thickness nm | processing | T_C K |
|--------|-----------------|-----------------|-------------------------|------------|
| A | 9 | 10 | <i>in situ</i> annealed | 153 |
| B | 8.5 | 14 | as grown | 127 |
| C | 10.5 | 20 | as grown | 95 |

in the magnetometer chamber [37]. A special demagnetization procedure has been employed to minimize the influence of trapped parasitic fields during near-zero-field measurements. As the most relevant measurements are gathered at weak magnetic fields in the “hard axis” configuration, we strictly follow the experimental code and data reduction detailed in Ref. [37]. All the data presented here have their relevant diamagnetic contributions evaluated at room temperature and subtracted adequately. The temperature dependence of remnant magnetization (TRM) measured along both cleaving edges of the sample ($\langle 110 \rangle$ directions for zinc-blende substrates) serves to obtain an overview of magnetic anisotropy as well as to determine T_C . To study the magnetic anisotropy in a greater detail, magnetic hysteresis loops $M(H)$ are recorded in an external magnetic field H in the range of ± 1 kOe along the same $\langle 110 \rangle$ in-plane directions. The SQUID studies are supplemented by the in-plane angular dependence of the FMR performed at selected temperatures at $\omega/2\pi = 9.3$ GHz. It is shown below that both methods yield consistent results.

III. EXPERIMENTAL RESULTS

A. Overview of magnetic anisotropy

There are few sources of magnetic anisotropy in (Ga,Mn)As epilayers: T_d symmetry of the crystal, the epitaxial strain, a preferential aggregation of Mn dimers along one direction, and the shape anisotropy caused by the demagnetization effect. Their sign and magnitude depend in turn on the ratio of valence-band splitting to the Fermi energy, and so varies substantially with an effective Mn concentration ($x_{\text{eff}} = x_{\text{sub}} - x_I$ [11], where x_{sub} is the concentration of substitutional Mn at Ga sites and x_I is the concentration of interstitially located Mn species Mn_I) and temperature (both determine the magnitude of M), epitaxial strain, and p . It has been generally accepted that in layers where the easy plane configuration is realized, two leading terms are sufficient to adequately describe magnetization processes. They are the crystal symmetry related, fourfold (cubic) component [8], and the Mn-dimer related uniaxial one [38,39]. So, the phenomenological description of the total in-plane magnetostatic energy of the system is usually taken as

$$E_m = \frac{K_C}{4} \sin^2 2\varphi + K_U \sin^2 \varphi - MH \cos(\varphi_H - \varphi), \quad (1)$$

i.e., assuming a single-domain behavior of a uniformly magnetized material. Here, K_C and K_U denote the lowest order cubic and uniaxial anisotropy constants, M is the saturation magnetization, and φ_H and φ are the angles of H and M to the $[100]$ direction. In its chosen form, Eq. (1) takes into account that both components are angled at $\pi/4$ to each other and that the positive sign of K_C represents $\langle 100 \rangle$ orientation of the easy axes of the cubic component. It also gives an account for easy \leftrightarrow hard axis switching represented here by a change of the sign of the relevant K . These are the $[1\bar{1}0] \leftrightarrow [110]$ $\pi/2$ rotations for the uniaxial term [3,40], and, for the very first time reported here, $\pi/4$ in-plane rotations, $\langle 100 \rangle \leftrightarrow \langle 110 \rangle$, of the cubic term. Additionally, since magnitudes of K_C and K_U are x_{eff} , p , and most importantly, T -dependent, so yet another in-plane SRT frequently takes place at temperature where $K_U = K_C$

[17]. This second-order magnetic SRT separates two different regimes. When $|K_C| < |K_U|$, as it is the case of the present study, (Ga,Mn)As acquires nearly perfect magnetic uniaxial properties. In such a case, the presence of a weaker cubic term modifies the uniaxial behavior only very little. In particular, it does not reveal its presence at $H = 0$, and so to reveal its properties an external magnetic field is required.

The relationship between the uniaxial hard axis magnetization $M_{[110]}$ and H is obtained by minimizing the energy given by Eq. (1) with respect to φ while setting $\varphi_H = \pi/4$:

$$HM = 2(K_U - K_C)\bar{m}_{[110]} + 4K_C\bar{m}_{[110]}^3, \quad (2)$$

where the reduced hard axis magnetization $\bar{m}_{[110]} = M_{[110]}/M$. The first term in Eq. (2), dominating when $\bar{m}_{[110]} \simeq 0$, that is, at very weak magnetic fields, describes the initial, linear in H , magnetization process which begins with a slope $s = M/(K_U - K_C)/2$. Here, the influence of the fourfold anisotropy is only quantitative. It redefines the magnitude of the initial slope of the otherwise linear response. However, it plays the decisive role at mid-field region (i.e., when $\bar{m}_{[110]} \rightarrow 1$) since it sets both the strength and the curvature of the nonlinear part of $\bar{m}_{[110]}(H)$. Accordingly, $\bar{m}_{[110]}(H)$ bends downwards for $K_C > 0$, exhibiting the typical concave character reported so far, but it will turn upwards exhibiting the *convex* curvature for $K_C < 0$. Actually, the initial reduction of s by negative K_C makes the convex curvature of $\bar{m}_{[110]}(H)$ a bit more pronounced, creating together an unmistakable fingerprint that the cubic easy axes attain $\langle 110 \rangle$ directions in the sample.

B. Experimental determination of anisotropy constants

The case of the convex curvature in $\bar{m}_{[110]}(H)$ is exemplified in Fig. 2 for sample A. Clearly, after a linear start, an up-turn is seen for $\bar{m}_{[110]}(H)$ taken at 50 K. Interestingly, at 80 K the $\bar{m}_{[110]}(H)$ remains linear in H nearly up to the full saturation, indicating that around this temperature the curvature changes

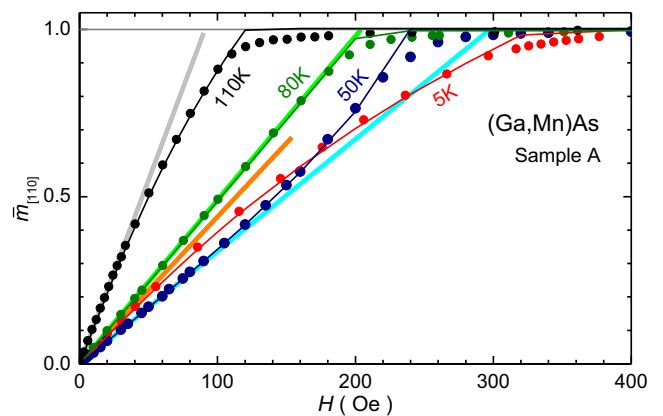


FIG. 2. Uniaxial hard axis magnetic isotherms $\bar{m}_{[110]}(H) = M_{[110]}(H)/M$ at selected temperatures for sample A (solid points) exemplifying different curvatures of mid-field part of the $m(H)$. The background thick lines of lighter shades indicate the initial slope of each $\bar{m}_{[110]}(H)$ and serve as references to ease the identification of the curvatures. The thin solid lines of matching colors are calculated from Eq. (2) treating the anisotropy constants as adjustable parameters.

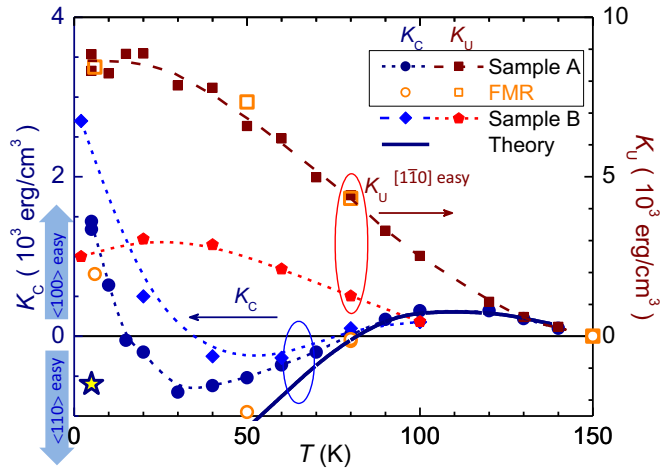


FIG. 3. Temperature dependence of uniaxial (K_U , squares and pentagons) and cubic (K_C , bullets and diamond) anisotropy constants. Solid points are obtained from analysis of uniaxial hard axis magnetization curves $\bar{m}_{[110]}(H)$ open ones are obtained from analysis of the angular dependence of FRM resonance positions. Dashed lines are guides for the eye only. In the notion adopted here, the positive/negative sign of K_C indicates that the cubic easy axes are aligned along $\langle 100 \rangle / \langle 110 \rangle$ directions, respectively. The star represents a low-temperature estimation of K_C after removal from the original $\bar{m}_{[110]}(H)$, a part attributed to nonhomogeneous magnetization originated at the interface regions, as detailed in Sec. V. Thick solid line represents results of the Zener mean-field model, including a Gaussian broadening of the density of states and a single-ion anisotropy contribution, as described in Sec. IV.

its sign, heralding the SRT of the cubic anisotropy at around this T . This fact is corroborated by a concave shape of $\bar{m}_{[110]}(H, 110\text{K})$. The existence of these different curvatures is highlighted in Fig. 2 by shaded thick background lines marking the initial slope of $\bar{m}_{[110]}(H)$ at these temperatures.

Interestingly, a similar to $T = 110\text{K}$ concave character of $\bar{m}_{[110]}(H)$ is seen at the lowest temperatures, exemplified in Fig. 2 for $T = 5\text{K}$. As argued above, to account for such $\bar{m}_{[110]}(H)$, a positive K_C is required, but it will be reasoned further in the text that the incorporation of the previously disregarded contribution from the SP-L component in the analysis of magnetization curves in (Ga,Mn)As may well lead to the same concave curvature.

A complete set of $M_{[110]}(H)$ curves obtained in a broad temperature range permits us to establish upon Eq. (2) the temperature dependence of the anisotropy constants in our samples. To this end, we take advantage that at each temperature both K_C and K_U are bound by the experimentally established magnitudes of M and the initial slope s . This constrain assures a perfect fit in the weak field region and reduces the whole analysis to a simple choice of K_C to reproduce the mid-field curvature of $\bar{m}_{[110]}(H)$ for the already fixed s . Such determined magnitudes of K_C and K_U are collected in Fig. 3. Interestingly, while exhibiting much lower amplitudes than K_U , the sign of cubic component clearly oscillates as a function of T . On lowering T , the first rotation $\langle 100 \rangle \rightarrow \langle 110 \rangle$ takes place at around 80 K, and a rotation back to $\langle 100 \rangle$ at much lower temperatures is suggested by the analysis.

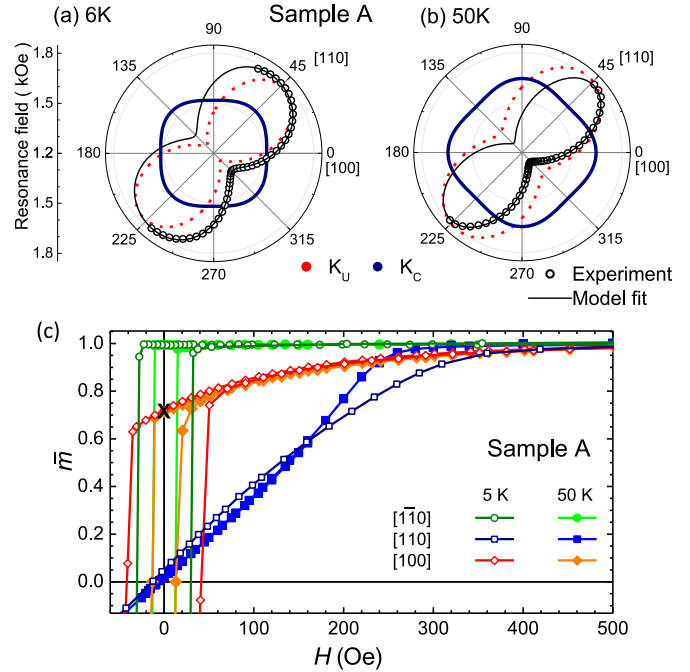


FIG. 4. Polar plot of the in-plane angular dependencies of the ferromagnetic resonance (open circles) and the established uniaxial (dotted red thick line) and cubic (navy thick line) contribution to the total magnetic energy for sample A at 6 (a) and 50 K (b). (c) Magnetic isotherms $\bar{m}(H) = M(H)/M$ measured for the same sample A along three major in-plane crystallographic orientations, $[1\bar{1}0]$ (circles), $[110]$ (squares), and $[100]$ (diamonds), at the same two temperatures [6 K (open) and 50 K (full symbols)]. A black cross at $H = 0$ and $\bar{m} = 1/\sqrt{2}$ marks the expected magnitude of remnant \bar{m} for the $[100]$ orientation in a single domain approach defined by Eq. (1) expected for $|K_C| < |K_U|$.

C. Ferromagnetic resonance

Both the negative sign at 50 K and a positive one at low T of K_C comes out from the FMR studies. In the top panels of Fig. 4, the dependence of the measured resonant fields on the orientation of the applied magnetic field is shown for the same sample A at 6 and 50 K (open circles). The resonant field is obtained by evaluating the standard Artman equation [41] at the equilibrium position of M ($\partial E_m / \partial \varphi = 0$) treating K_C and K_U as fitting parameters. The thin solid lines in panels (a) and (b) in Fig. 4 show the established dependency of the resonant fields on φ_H along with its decomposition into uniaxial (dotted red thick line) and cubic (dark thick line) contributions. The extracted magnitudes of K_C and K_U are presented in Fig. 3 (open symbols) exhibiting a perfect correspondence to the results obtained from magnetization studies presented in the bottom panel of Fig. 4. Again, analyzing the data within the frame set by Eq. (1), a suggestive picture that the cubic anisotropy changes sign at the lowest temperatures is obtained.

D. Dependence on hole density

Having established that the cubic easy axes can acquire $\langle 110 \rangle$ in-plane directions in (Ga,Mn)As we can now turn to a more fundamental question of the role of hole density. To this end, we subject sample C to incremental open air LT annealing

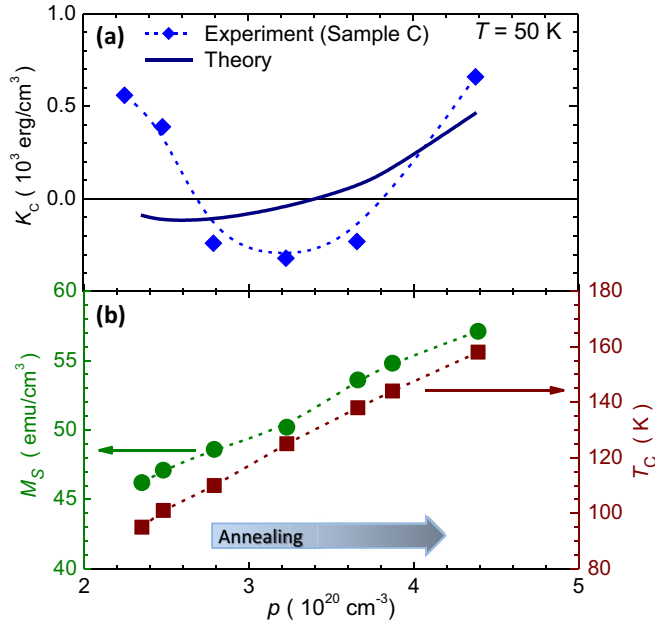


FIG. 5. (a) Hole density p dependence of cubic anisotropy constant (K_C , diamonds) established during incremental low-temperature annealing. The magnitudes of p at each annealing step are obtained from modeling of the corresponding experimental values of Curie temperature T_C and saturation magnetization M_S determined during annealing (b). Dashed line in (a) is a guide for the eye only. Thick solid line represents results of the mean-field Zener model with a Gaussian broadening of the density of states and a single-ion anisotropy contribution included, as detailed in Sec. IV.

[42,43], since the corresponding out-diffusion and surface passivation of Mn_I increases p [44]. We perform the annealing in small steps at progressively increasing temperatures (from 150 °C to 180 °C) and annealing times: from 1 to 36 h. To assess the changes in electrical and micromagnetic properties caused by the annealing, the full suite of magnetic measurements is performed after each annealing step.

Knowing the sample's T_C and saturation magnetization $M_S = x_{\text{eff}} N_0 g \mu_B S$ at each annealing step [depicted in Fig. 5(b)], the corresponding hole density $p = N_0(3x_{\text{eff}} - x)/2$ is readily obtained in the framework of the mean-field p - d Zener model, treating the problem in a self-consistent way by the incorporation of hole contribution to M_S calculated for the same x_{eff} [7,8]. It is assumed here that the only hole compensating defect is the double charged interstitial donor and that $x_{\text{eff}} = x_{\text{sub}} - x_I$ [11]. $N_0 = 2.21 \times 10^{22} \text{ cm}^{-3}$ is the cation concentration in GaAs, $S = 5/2$ is the Mn spin, $g = 2.0$, and μ_B is the Bohr magneton. We confirm that with fixed $x_{\text{sub}} = 9.3\%$ this procedure allows us to reproduce exactly the experimentally established magnitudes of T_C within 10% margin for M_S . The established at 50 K magnitudes of K_C are plotted as a function p in Fig. 5(a), clearly indicating an oscillatory dependence of K_C on p . Remarkably, this is qualitatively the dependence that is predicted by the mean-field p - d Zener model [8], however, contradictory to the model calculations (cf., Fig. 9 in Ref. [8]), the negative dip in $K_C(p)$ is much shallower and spans a narrower band in p .

IV. THEORETICAL MODELING

Undoubtedly, the overall qualitative agreement between the experimental findings and the theory of DFS based on the p - d Zener model presented here constitutes a great leap toward a reconciliation of experiment and model predictions. On the other hand, the noted quantitative discrepancies call for a more in-depth reexamination of both the experimental and theoretical approaches.

We start our attempt from the theoretical side and introduce two ingredients to the standard theory of magnetic anisotropy in DFSs [1,4]. First, we consider how scattering-induced broadening of density of states affects the amplitude of cubic magnetic anisotropy as a function of the hole concentration. Second, we examine the role of single-ion magnetic anisotropy. Our results demonstrate that the disorder-induced reduction in the magnitude of carrier-mediated magnetic anisotropy opens the floor for single-ion anisotropy despite the relatively small magnitude of the latter for Mn ions in orbital singlet state. These two effects work together and elucidate why the $\langle 100 \rangle$ orientation of the easy axis is more frequently observed experimentally.

A. Disorder effects

In order to describe effects of disorder associated, in particular, with the presence of randomly distributed ionized Mn acceptors, we incorporate into the p - d Zener model of magnetic anisotropy a Gaussian broadening of hole energy states, the procedure employed previously in studies of Curie temperatures in p -(Cd,Mn)Te quantum wells [45]. As shown in Fig. 6, such an approach predicts a reduction in the amplitude of the cubic anisotropy energy. This reduction is already twofold for the standard deviation $\sigma = 40$ meV, i.e., for the lower bound value expected for the lifetime energy broadening, typically, comparable to the Fermi energy in (Ga,Mn)As [1]. A decrease in the magnitude of the carrier-mediated term enhances the relative importance of single-ion magnetic anisotropy.

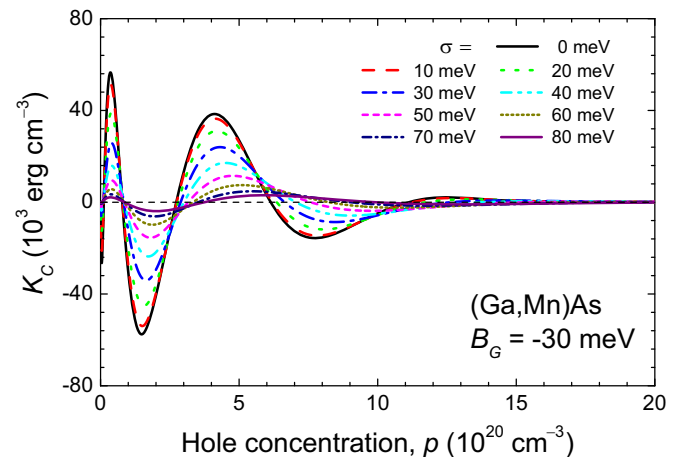


FIG. 6. The effect of disorder on the magnitude of the carrier-mediated in-plane cubic anisotropy coefficient K_C computed within the mean-field p - d Zener model extended by including a Gaussian broadening of the hole energy states for various values of the standard deviation σ .

B. Single-ion magnetic anisotropy

The cubic anisotropy of a single Mn spin with $S = 5/2$ is described by the Hamiltonian

$$\mathcal{H}_{\text{SI}} = \frac{a}{6} \left[S_x^4 + S_y^4 + S_z^4 - \frac{S(S+1)(3S^2+3S-1)}{5} \right], \quad (3)$$

where, according to electron paramagnetic resonance studies, $a \simeq -2.85 \times 10^{-19}$ erg in GaAs:Mn [46,47]. The negative sign of a implies the orientation of the cubic easy axes along the $\langle 100 \rangle$ family of crystallographic directions.

In order to determine the magnitude of single-ion magnetic anisotropy in the low-temperature limit, we calculate the expectation values $E_S^{\text{SI}}(\theta, \varphi)$ of \mathcal{H}_{SI} in the spin coherent states $|\psi_S^{\text{SC}}(\theta, \varphi)\rangle$,

$$E_{5/2}^{\text{SI}}(\theta, \varphi) = \frac{4a}{125} \left[\langle S_x \rangle^4 + \langle S_y \rangle^4 + \langle S_z \rangle^4 - \frac{375}{16} \right]. \quad (4)$$

This expression represents the lowest order cubic anisotropy energy and for noninteracting Mn spins leads to the in-plane anisotropy coefficient,

$$K_C^{\text{SI}} = x_{\text{eff}} 15.6 \times 10^3 \text{ erg/cm}^3. \quad (5)$$

As seen by comparing Eqs. (3) and (4), the low-temperature quantum limit of K_C^{SI} is about five times reduced with respect to the value expected for the classical vector $S = 5/2$.

We are interested in the role played by single-ion magnetic anisotropy in the case of ferromagnetic (Ga,Mn)As, i.e., in the presence of the hole liquid. In order to evaluate the magnitude of K_C^{SI} in such a case, we take the magnetization vector \mathbf{M} of Mn spins as an order parameter and consider the Landau-Ginzburg free energy functional in the form containing the Mn contribution in the absence of carriers and the carrier term [1],

$$\mathcal{F}(\mathbf{M}) = \mathcal{F}_S(\mathbf{M}) + \mathcal{F}_c(\mathbf{M}), \quad (6)$$

where

$$\mathcal{F}_S(\mathbf{M}) = \int_0^{\mathbf{M}} d\mathbf{M}_o \cdot \mathbf{h}(\mathbf{M}_o) - \mathbf{M} \cdot \mathbf{H}. \quad (7)$$

Here, $\mathbf{h}(\mathbf{M}_o)$ denotes the inverse function to $\mathbf{M}_o(\mathbf{h})$, where \mathbf{M}_o is the magnetization of Mn spins in the absence of carriers in the field \mathbf{h} and temperature T computed from the single-ion spin Hamiltonian given in Eq. (3), supplemented by the Zeeman term $-g\mu_B \mathbf{h} \cdot \mathbf{S}$.

Now, we are in position to evaluate $\mathcal{F}_S(\mathbf{M})$ as a function of M for two azimuthal angles $\varphi = 0$ and $\pi/4$ as a series expansion in M assuming that a is small. The resulting values of K_C are shown in Fig. 7.

To conclude this section, we compare in Fig. 3 the experimental data with a theoretical result obtained within the extended Zener model, discussed above. In these computations, $p = 3.3 \times 10^{20} \text{ cm}^{-3}$, as inferred from the magnitudes of T_C and M_S of sample A. Furthermore, we assume $\sigma = 70 \text{ meV}$ in order to reproduce the experimental magnitude of K_C in the high-temperature region. The divergence between the theoretical and experimental data visible at $T \rightarrow 0$ indicates that at $x_{\text{eff}} \simeq 7\%$ the single-ion anisotropy is too weak to overcome a large carrier liquid contribution and to explain the sign change of K_C inferred experimentally at low temperatures. On the other hand, choosing a higher value of σ allows to

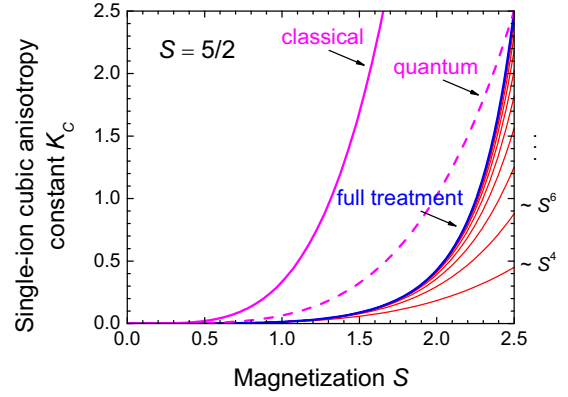


FIG. 7. Single-ion cubic anisotropy coefficient for noninteracting $S = 5/2$ spins as a function of magnetization $\langle S \rangle$, in units of $-a$. The curve designated “classical” represents evaluation treating S as a classical vector, while the dashed curve “quantum” is rescaled by the factor of $24/125$ to match the low-temperature limit of the quantum calculation. “Full treatment” corresponds to the mean-field approach to the ferromagnetic case [Eq. (7)]. The thin red curves represent consequent orders of expansion in powers of magnetization, while the blue thick curve has been obtained by the Aitken extrapolation.

reproduce this change of sign but the resulting magnitude of $|K_C|$ is much smaller than the experimental values.

V. THE INTERFACE CONTRIBUTION

Maybe such stringent measures are not really required and the need to reproduce the second, the low- T change of sign of K_C is largely apparent. We note here that the magnitudes of both anisotropy constants, although technically obtained in a correct way, are established upon a very strong assumption of a perfect magnetic uniformity of (Ga,Mn)As, the sole condition under which Eq. (1) is valid. In this section we present a method of the experimental assessment of the previously disregarded contribution in the micromagnetic consideration of (Ga,Mn)As brought about by the magnetic phase separation driven by electrostatic inhomogeneities specific to the proximity of metal-insulator transition (MIT).

We start from the notion that there has been a growing number of experimental evidences that this SP-L contribution assumes even a dominant role, determining the magnetic properties of low and very low- x samples. There, a low magnitude of p is guaranteed by a weak Mn doping [48–50]. More importantly, in structures with a much higher x similarly low magnitudes of p may result from intentional or unintentional drainage of holes out of the DFS [27,29,51,52]. In particular, in (Ga,Mn)As layers, such a situation takes place at the vicinity of the free surface and near the interface with an n -type LT-GaAs buffer. Two space-charge layers formed at these limits sizably deplete both (Ga,Mn)As edges, forcing localization of carriers which in DFS mediate the FM order. According to the two-fluid model of electronic states in the vicinity of the Anderson-Mott MIT [53], it will be either a weak or a strong localization, depending on the degree of depletion. This electrical disorder, via enhanced local density fluctuations, sets the ground for a magnetic nanoscale phase separation [30,31]. In such an environment, the FM order

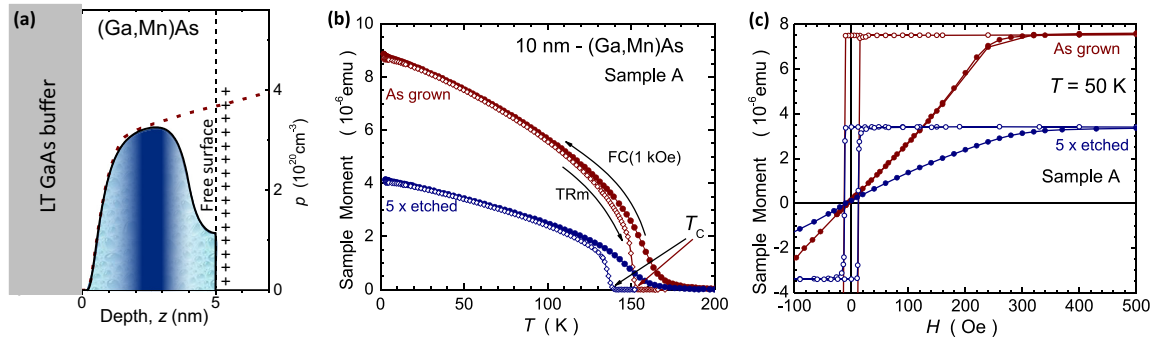


FIG. 8. (a) Thick black line: expected vertical hole density profile $p(z)$ for the $d = 5 \text{ nm}$ thin (Ga,Mn)As layer. The dashed line indicates the first 7-nm $p(z)$ in the original (Ga,Mn)As layer before thinning. An excerpt from Fig. 3(a) in Ref. [28]. The dark shaded part of the profile marks the central part of the layer where uniform ferromagnetic coupling specific to metallic (Ga,Mn)As prevails. On moving away towards the interfaces, the rapidly decreasing p results in the magnetic phase separation, as indicated by a light blue texture. (b) Temperature T and (c) magnetic field H dependent studies of the same samples. The thermoremanent moments (TRm) are acquired for the uniaxial easy orientation (along $[1\bar{1}0]$) on warming after field cooling the samples at $H = 1 \text{ kOe}$ to about 2 K and quenching H to sub-Oe range. Arrows indicate the magnitudes of Curie temperature T_C established upon TRm. H -dependent characteristics for $T = 50 \text{ K}$ are shown for both uniaxial easy ($[1\bar{1}0]$: open symbols) and hard axis ($[110]$: full symbols) orientations.

gets constrained to mesoscopic lengths, being maintained only within these fragments, which are visited by (weakly) localized holes. These small FM volumes exert (as an ensemble) SP-L properties and introduce magnetic features characteristic to a dynamical slow down due to activated processes in the presence of energy barriers and, most importantly for this study, a concave curvature of their Langevine-like magnetic isotherms $m_{\text{SP-L}}(H)$ is added to the magnetic response of the remaining metallic part of the sample.

The importance of SP-L admixture depends on the volumetric ratio of the mesoscopic to long-range parts of the sample, so it has to be sizable in very thin layers, in particular when effects in time domain [29] or dependent on the curvature of $M(H)$ are probed. In a broad view, the following aspects have to be taken into consideration. Firstly, because (Ga,Mn)As is at the vicinity of MIT, it does not take much to impose the magnetic disorder due to local fluctuation of p in samples with uniform Mn distribution and flat interfaces [27,30,54,55]. Secondly, even crystallographically best and uniformly Mn-doped layers have got two limiting surfaces where the hole depletion is likely to occur. Therefore SP-L effects are expected to surface to a certain degree in every (Ga,Mn)As layer. Thirdly, the formation of the SP-L disorder is expected not only at low T . Since $T_C \propto x$ in DFS, the magnetic phase separation may already start even at moderate temperatures at the edges of large x samples. It may actually persist up to a significant fraction of T_C for high quality (optimally annealed) films, or, more generally, up to temperatures comparable to, or even exceeding, T_C in electrically compensated samples [29]. Lastly, and sadly, the details of the magnetic characteristics of this SP-L component are not exactly known, so they cannot be correctly included in the magnetostatic energy considerations even on a phenomenological level. Therefore the analysis of the experimentally established quantities, either as a function of magnetic field, temperature, or time are no longer expected to yield correct results when it is based on the assumption of the “ideal,” magnetically homogenous material, as exemplified recently in the case of Gilbert damping constant study in (Ga,Mn)As [29].

Below, we present our attempt to assess the low- T magnitude of the “interface-born” SP-L magnetic moment $m_{\text{SP-L}}(H)$ in 10-nm-thin sample A. Then, basing on some heuristic arguments, we show that indeed a presence of such a contribution does revert the sign of the otherwise negative cubic anisotropy constant if the analysis of the magnetic data collected here is based on the time honored approach [Eq. (1)], originally put forward for an idealistic homogenous “edgeless” (Ga,Mn)As. Such a profound influence on the results of the analysis is brought about by the same concave curvature of both the Langevine-like $m_{\text{SP-L}}(H)$ and the cubic anisotropy contribution in (Ga,Mn)As for $K_C > 0$, as already detailed in Sec. III A.

To evaluate the magnitude of $m_{\text{SP-L}}(H)$, we use the concept of fine thinning of (Ga,Mn)As by multiple etching of the native oxide in HCl [28,56,57]. In particular, we note, following the vertical hole density profile $p(z)$ established upon the same thinning procedure as in a similar (Ga,Mn)As layer (cf. Fig. 3(a) in Ref. [28]) that by reducing the layer thickness d down to about 5 nm we should be left only with a marginally thin (1–2 nm), high hole density mid-part (slab) of the initial layer, sandwiched between two edge layers (approximately 1.5 nm each) with sizably reduced p , as sketched in Fig. 8(a). Importantly, to assess the role of SP-L component in the initial layer, we need only just such a thin layer that (i) it can be regarded as consisting mostly of “two edges” (the top one at the free surface and the bottom one at the interface with the n -type LT GaAs buffer), but that (ii) it remains thick enough to avoid too strong depletion, not present in the original, 10-nm layer. In our understanding, it is the presence of this $\sim 1+$ nm thin high- p central part which guarantees this correspondence. It needs to be added here that the thinning of the initially studied layer assures us that we deal with the same material as the originally investigated. Resorting to other, deliberately grown 5-nm layers would greatly reduce the relevance of this exercise as different magnitudes of x_{eff} and p and/or their different volume distribution are likely.

The effect of etching on magnetic properties is presented in Figs. 8(b) and 8(c) where basic T and H characteristics are plotted for the original 10-nm sample A and after 5 consecutive

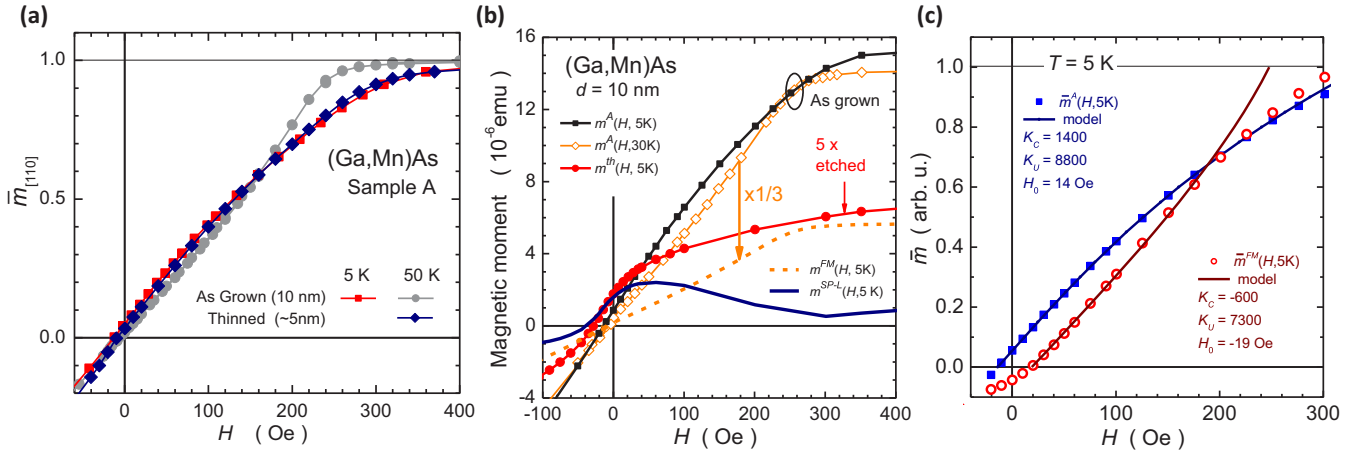


FIG. 9. (a) Comparison of the changes to $T = 50$ K uniaxial hard axis magnetic isotherm $\bar{m}_{[110]}(H) = M_{[110]}(H)/M$ (grey bullets) due to lowering temperature to 5 K (red squares) and thinning the layer down to 5 nm (navy diamonds). (b) Illustration of the method used to establish low temperature magnetic field H response specific to interfaces in 10 nm thin sample A (the thick navy line). All measurements are performed along $[110]$, the uniaxial hard direction. The labeling of the data sets corresponds to the notation used in the text. (c) The same sample. A comparison between the original hard axis magnetization curve (solid squares) and the specific to ferromagnetic (uniform) part of the sample (open circles). The background thick lines of lighter shades indicate the initial slope of each $\bar{m}(H)$ and serve as references to ease the identification of the opposite mid-field curvatures. The solid lines of matching colors represent the modeling of the data by Eq. (2). The magnitudes of the established uniaxial K_U and cubic K_C anisotropy constants are denoted in the panel (in units of erg/cm³), together with values of a required extra horizontal shift H_0 to align modeled curves with the experimental points at $m(H) \simeq 0$.

etchings. After each etching, the sample has been left at an ambient atmosphere for at least a day to assure a maximum in-diffusion of oxygen and a full oxidation of the topmost ~ 1 nm of the layer. The magnitude of the drop of the signal registered in Fig. 8 provides also a scaling factor pointing to the intended ~ 5 –nm final thickness after etching. The T_C of the thinned layer dropped in comparison to the original sample by about 13 K, a number consistent with the reduction reported in Ref. [28] at the same range of thicknesses, substantiating the use of the finding established there. Another worth mentioning feature of the magnetic data in Fig. 8 is the excellent uniaxial behavior exhibited also after thinning. This shows that after the full five cycles of etching and oxidations, the central part of the layer preserved its pristine micromagnetic properties specific to the homogeneous (Ga,Mn)As.

On the other hand, it is evident that upon thinning the curvature of $m_{[110]}(H)$ at $T = 50$ K has changed in a very similar way as it did upon lowering T to 5 K in the original sample before thinning (cf. Fig. 2). In fact, the similarities are striking and seen best when both these hard axis magnetization curves are plotted in one graph in relative units, see Fig. 9(a). Although not being a definitive proof, this finding very strongly supports our original conjecture that depleted regions in (Ga,Mn)As are the source of SP-L contribution to magnetization and either a sufficiently low temperature or a sizably diminished volume of the FM part or both are needed to make this contribution relevant.

Now, having established this thinning \leftrightarrow lowering- T correspondence, we will evaluate the magnitude of $m_{SP-L}(H)$ in the original sample A at 5 K and show that indeed its presence in real systems may sizably influence the determination of anisotropy constants if the data analysis is based only on a single-domain model with a uniform magnetization throughout the layer. Our method is based upon the three following assumptions. Firstly, both the FM and the SP-L components

can be treated additively [27]. Secondly, after thinning to 5 nm, the depleted volumes take up about $f = 2/3$ of the whole volume of the thinned layer. This is taken from the $p(z)$ profile presented in Fig. 8(a). Thirdly, the thinning has a little effect on $m_{SP-L}(H)$. Indeed, the bottom interface does not change at all and the long oxidation time after etching assures a very similar depletion zone near the free surface. Therefore the observed changes of the magnitude and the character of the experimental $m_{[110]}(H)$ are solely due to the sizable reduction of the contribution brought about by the FM part. However, to evaluate the magnitude of $m_{SP-L}(H)$ with a reasonable confidence, a model of the low- T $m_{[110]}(H)$ specific to the FM part is needed. Obviously, a scaled down $m_{[110]}(H)$ of the original sample A should serve for this purpose, but to minimize the contribution of the SP-L component it cannot be taken from too low T . Nonetheless, it should not be taken either from a too high T —to correspond as close as possible to the “ideal” low- T magnetic response of the FM part of the sample, presumed here to be characterized by a negative K_C . At this point, a choice has to be made and upon the inspection of the data presented in Fig. 3 it appears that for the sample A the most suitable reference $m_{[110]}^{\text{ref}}(H)$ should be that one measured at $T = 30$ K, since the values of K_C established at higher temperatures for this sample stop growing more negative on lowering T just about 30 K.

Corresponding uniaxial hard axis magnetization curves measured at 5 K for sample A $m_{[110]}^A(H, 5\text{ K})$ and after thinning $m_{[110]}^{\text{th}}(H, 5\text{ K})$ are presented in Fig. 9(b) (full symbols), indicating, similarly to 50 K, a more concave character of $m_{[110]}(H)$ of the thinned layer. On the other hand, the added to this figure $m_{[110]}^{\text{ref}}(H)$ [that measured at 30 K for the same sample (open diamonds)], in accordance with the data presented in Figs. 2 and 3, exhibits a convex curvature. However, in the etched layer, this response should be exerted by about

(1 - f), i.e., a third of its volume, so by scaling it down three times [the dashed line in Fig. 9(b)] and subtracting from $m_{[110]}^{\text{th}}(H, 5 \text{ K})$ we obtain the required experimental estimation of the SP-L contribution to $m(H)$ at 5 K, $m_{[110]}^{\text{SP-L}}(H, 5 \text{ K})$, marked as the thick solid line in Fig. 9(b). The magnitude of $m_{[110]}^{\text{SP-L}}(H, 5 \text{ K})$ is rather weak, particularly when compared to the saturation values of $m_{[110]}^{\text{A}}(H, 5 \text{ K})$, so it could be regarded as a secondary contribution to any leading characteristics of the material. However, and in accordance to our expectations, this $m_{[110]}^{\text{SP-L}}(H, 5 \text{ K})$ exhibits a very strong concave curvature at weak magnetic fields, and so the presence of such a contribution sizably impairs the determination of K_C .

Having evaluated the SP-L contribution, we are in position to calculate the FM response of sample A at 5 K, i.e., as it would be if the sample had not had depleted regions near its interfaces $m_{[110]}^{\text{FM}}(H, 5 \text{ K}) = m_{[110]}^{\text{A}}(H, 5 \text{ K}) - m_{[110]}^{\text{SP-L}}(H, 5 \text{ K})$. The original and calculated $m(H)$ are plotted in Fig. 9(c) in relative units \bar{m} , marked by full and open symbols, respectively. Thick solid lines of lighter shades represent their initial slopes (established around $\bar{m} \simeq 0$) and guide the eyes to indicate the opposite curvatures of both dependencies in the mid-field region. Importantly, the new $\bar{m}(H)$, $m_{[110]}^{\text{FM}}(H, 5 \text{ K})$, exhibits now a clear *upward* shift in the mid-field range, which according to the general model of magnetic anisotropy in (Ga,Mn)As [Eq. (2)] corresponds to a negative K_C . We can now evaluate its magnitude using the same method as employed before in Sec. III B. The obtained this way magnitude of $K_C^*(5 \text{ K}) = -600 \text{ erg/cm}^3$, represented in Fig. 3 by a star, is most likely still far from being a precise one, but is undoubtedly opposite to that one established from the analysis of bare $\bar{m}_{[110]}^{\text{A}}(H, 5 \text{ K})$, and it corresponds much better to the expectations brought about by the elaborated in the previous section extended Zener model of FM in (Ga,Mn)As. It needs to be added that the final outcome of our procedure—the negative sign of K_C^* —does not depend on the exact choice of (1 - f) from 0.25 to 0.5.

We are now turning our attention back to the FMR data, which at the very moment may seem to contradict the last finding. However, this does not have to be the case. First of all, as already established by some of the present authors [27], the SP-L volumes exhibit well defined uniaxial anisotropy which is perpendicular to that exerted by the FM part of such layers as investigated here, i.e., along [110]. Therefore their effective moments point predominantly in that direction and their effective fields sum up at low T . This has to be the case, since the FMR line remains as narrow at 6 K as it is at 50 K, despite the presence of such local fields. However, the presence of this coherent effective field has to modify the resonance condition, and most probably it is done in a way that the resulting angular dependence, still very uniaxial-like, acquires a term that corresponds to an effective cubic component which is rotated by about $\pi/4$ with respect to that originating from the magnetically uniform part of the layer. In fact, in the FMR experiment, an additional absorption is seen at weak fields but it remains to be seen whether it can be connected with these magnetically separated volumes.

We finally comment on the strangely negative values of $\bar{m}_{[110]}^{\text{FM}}(H, 5 \text{ K})$ at $H \simeq 0$ [Fig. 9(c)]. In our view, this is a result of yet another characteristic feature of the inhomogeneous constitution of (Ga,Mn)As. We do not elaborate on this issue here, it is a subject of an in-depth independent study. We

remark only that when (Ga,Mn)As is measured within the parameter space corresponding to the formation of SP-L phase, this fragment of $M(H)$ where the magnetization reversal takes place is strongly dependent on the rate at which the magnetic field is swept, particularly at low T [58], which is a characteristic feature of the dynamical slow down due to activated processes in the presence of energy barriers. Since thinning and/or electrical compensation in (Ga,Mn)As promotes a growth of f towards unity, a low- T increase of experimentally established coercivity H_C is indeed expected in thinned samples. This enlargement can be noticed in Fig. 9(b) for $m_{[110]}^{\text{th}}(H, 5 \text{ K})$ and it is this enlarged coercivity with respect to the more homogeneous sample A at 5 and 30 K that is the source of the slight down-shift of $m_{[110]}^{\text{FM}}(H, 5 \text{ K})$. Actually, the rapidly growing magnitude of H_C upon further thinning (not shown) is the source of the second (practical) reason why the evaluation of SP-L contribution stopped at 5 nm. Nevertheless, even in such a case, the magnitudes of anisotropy constants can be still evaluated within the frame of the method described in Sec. III B by introducing an artificial extra parameter allowing us to align the modeled by Eq. (2) $\bar{m}_{[110]}(H)$ with the experimental points at $\bar{m}(H) = 0$.

We summarize this section by noting why the $\langle 110 \rangle$ cubic easy axes in (Ga,Mn)As might had gone unnoticed before. Surely, as with all the physical properties of DFS the samples must have the right magnitudes of p , T , and x_{eff} to grant an adequate balance of the relevant terms describing the free energy of the system. Secondly, as shown just above, the sample must be of a high magnetic uniformity to suppress the detrimental for “negative K_C ” contribution from the SP-L phase, at least, in not too thin layers and/or having strongly reduced interface depletion. But it is highly unlikely that our samples are the first that meet the criteria pointed above. So, we want to turn the attention to a far more down-to-earth reason: the details of experimental procedure. As presented in the study, the $\langle 110 \rangle$ cubic easy axes have been observed exclusively for not-fully annealed samples (i.e., in the middle of a small step annealing process) and at temperatures above 15 K and well below T_C , which is outside the envelope of typical conditions at which (Ga,Mn)As is tested or investigated. For example, a typical assessment of saturation magnetization is made at $T \leq 5 \text{ K}$. Here, the SP-L contribution really gets strength. On the other hand, T_C is frequently established from thermomnant measurements, which do not hint on the exact orientation of the cubic easy axes particularly at $T \rightarrow T_C$, where $|K_C| < |K_U|$. So, it is very likely that the existence of the negative K_C in (Ga,Mn)As might have been simply overlooked due to a too routine approach to the material characterization.

VI. CONCLUSIONS

Magnetic anisotropy of carefully prepared high quality thin layers of (Ga,Mn)As have been studied as a function of temperature and hole concentration both experimentally and theoretically. On the account of magnetic and ferromagnetic resonance studies it has been convincingly evidenced that within a certain range of p and T parameter space the cubic component to the in-plane magnetic anisotropy assumes the $\langle 110 \rangle$ easy axes. Accordingly, outside this frame, the cubic anisotropy reverts to ubiquitously reported $\langle 100 \rangle$ directions,

indicating an oscillating dependence of anisotropy constant on p and T . These features observed for the very first time qualitatively confirm the relevant predictions of the p - d Zener model of ferromagnetism in dilute ferromagnetic semiconductors [7], which can be taken as strong experimental support for the model. In particular, even a quantitative agreement has been obtained in the high- T and high- p part of the data when the more advanced form of the model developed here, which takes both the single-ion magnetic anisotropy of Mn species and the disorder into account, is applied. However, even in this advanced form the model cannot quantitatively reproduce the low- p and low- T rotation back of the easy axis to $\langle 100 \rangle$ orientations. We establish, however, that in these regimes, the magnitude and the sign of K_C determined upon the single-domain model with a uniform magnetization might be fraught with an error brought about by the magnetic phase separation into ferromagnetic and superparamagnetic-like regions. The phase separation, in turn, is driven by the electrostatic disorder specific to the proximity of the metal-insulator transition, particularly in interfacial regions of the layers in which the hole liquid is depleted and, thus, prone to localization. The key point of our reasoning is that the Langevine-like superparamagnetic response, by introducing the same concave curvature of the magnetization curves as is expected for the $\langle 100 \rangle$ oriented cubic term, forces any data analyzing procedure to yield more positive values for K_C than it would be obtained in the absence of this contribution. To substantiate our claims, we have presented an experimental procedure that allows to assess the magnitude of this detrimental superparamagnetic contribution to $m(H)$, and after correcting the bare experimental data, it has been shown that indeed the negative sign of K_C is obtained in accordance with the model computations.

Our results substantiate, therefore, the importance of the interfaces in the understanding of physical processes that take place in thin layers of DFS, and (Ga,Mn)As in particular. Despite the fact that it has been known for some time now [26,27,29], this study shows how the effects induced by interfacial depletion in (Ga,Mn)As preclude the correct determination of very relevant and important magnetic properties of the very thin samples. Importantly, the electrical disorder may well turn to be a dominant factor, also as a volume-born contribution to magnetism of DFS. Its importance has already been shown in electrically compensated and characterized by low magnitude of T_C/x ratio samples [29]. It plays even a decisive role in the determination of the magnetic response in very low Mn content (III,Mn)V samples [48–52]. Interestingly, whereas the electrical disorder, particularly in electrically compensated samples, was originally expected to smooth out the oscillatory behavior of the cubic anisotropy [8], the present findings point out to a new mechanism by which the electrical inhomogeneity affects the magnetic constitution of DFS.

ACKNOWLEDGMENTS

This study has been supported by the National Science Centre (Poland) through PRELUDIUM Grant No. UMO - 2012/05/N/ST3/03147 and MAESTRO Grant No. UMO - 2011/02/A/ST3/00125. EC Network SemiSpinNet (PITN-GA-2008-215368) contribution is also acknowledged. The International Centre for Interfacing Magnetism and Superconductivity with Topological Matter project is carried out within the International Research Agendas programme of the Foundation for Polish Science co-financed by the European Union under the European Regional Development Fund.

-
- [1] T. Dietl and H. Ohno, Dilute ferromagnetic semiconductors: Physics and spintronic structures, *Rev. Mod. Phys.* **86**, 187 (2014).
 - [2] H. Ohno, D. Chiba, F. Matsukura, T. Omiya, E. Abe, T. Dietl, Y. Ohno, and K. Ohtani, Electric-field control of ferromagnetism, *Nature (London)* **408**, 944 (2000).
 - [3] D. Chiba, M. Sawicki, Y. Nishitani, Y. Nakatani, F. Matsukura, and H. Ohno, Magnetization vector manipulation by electric fields, *Nature (London)* **455**, 515 (2008).
 - [4] T. Jungwirth, J. Wunderlich, V. Novák, K. Olejník, B. L. Gallagher, R. P. Campion, K. W. Edmonds, A. W. Rushforth, A. J. Ferguson, and P. Němec, Spin-dependent phenomena and device concepts explored in (Ga,Mn)As, *Rev. Mod. Phys.* **86**, 855 (2014).
 - [5] F. Matsukura, Y. Tokura, and H. Ohno, Control of magnetism by electric fields, *Nat. Nano.* **10**, 209 (2015).
 - [6] J. G. Alzate, P. K. Amiri, P. Upadhyaya, S. S. Cherepov, J. Zhu, M. Lewis, R. Dorrance, J. A. Katine, J. Langer, K. Galatsis, D. Markovic, I. Krivorotov, and K. L. Wang, in *IEEE International Electron Devices Meeting (IEDM), 10-13 December 2012, San Francisco, CA* (IEEE, Piscataway, 2012), pp. 29.5.1–29.5.4.
 - [7] T. Dietl, H. Ohno, F. Matsukura, J. Cibert, and D. Ferrand, Zener model description of ferromagnetism in zinc-blende magnetic semiconductors, *Science* **287**, 1019 (2000).
 - [8] T. Dietl, H. Ohno, and F. Matsukura, Hole-mediated ferromagnetism in tetrahedrally coordinated semiconductors, *Phys. Rev. B* **63**, 195205 (2001).
 - [9] T. Jungwirth, J. Sinova, J. Mašek, J. Kučera, and A. H. MacDonald, Theory of ferromagnetic (III,Mn)V semiconductors, *Rev. Mod. Phys.* **78**, 809 (2006).
 - [10] J. Zemen, J. Kučera, K. Olejník, and T. Jungwirth, Magnetocrystalline anisotropies in (Ga,Mn)As: Systematic theoretical study and comparison with experiment, *Phys. Rev. B* **80**, 155203 (2009).
 - [11] W. Stefanowicz, C. Śliwa, P. Aleshkevych, T. Dietl, M. Döppe, U. Würstbauer, W. Wegscheider, D. Weiss, and M. Sawicki, Magnetic anisotropy of epitaxial (Ga,Mn)As on (113)A GaAs, *Phys. Rev. B* **81**, 155203 (2010).
 - [12] A. Werpachowska and T. Dietl, Effect of inversion asymmetry on the intrinsic anomalous Hall effect in ferromagnetic (Ga,Mn)As, *Phys. Rev. B* **81**, 155205 (2010).
 - [13] A. Werpachowska and T. Dietl, Theory of spin waves in ferromagnetic (Ga,Mn)As, *Phys. Rev. B* **82**, 085204 (2010).
 - [14] H. Keça, V. K. Le, C. M. Brown, M. Sawicki, J. K. Furdyna, T. M. Giebułtowicz, and T. Dietl, Probing Hole-Induced Ferromagnetic Exchange in Magnetic Semiconductors by Inelastic Neutron Scattering, *Phys. Rev. Lett.* **91**, 087205 (2003).
 - [15] M. Sawicki, F. Matsukura, T. Dietl, G. M. Schott, C. Rüster, G. Schmidt, L. W. Molenkamp, and G. Karczewski, Temperature

- peculiarities of magnetic anisotropy in (Ga,Mn)As: The role of the hole concentration, *J. Supercond. Novel Magn.* **16**, 7 (2003).
- [16] M. Sawicki, F. Matsukura, A. Idziaszek, T. Dietl, G. M. Schott, C. Ruester, C. Gould, G. Karczewski, G. Schmidt, and L. W. Molenkamp, Temperature dependent magnetic anisotropy in (Ga,Mn)As layers, *Phys. Rev. B* **70**, 245325 (2004).
- [17] K.-Y. Wang, M. Sawicki, K. W. Edmonds, R. P. Campion, S. Maat, C. T. Foxon, B. L. Gallagher, and T. Dietl, Spin Reorientation Transition in Single-Domain (Ga,Mn)As, *Phys. Rev. Lett.* **95**, 217204 (2005).
- [18] M. Glunk, J. Daeubler, L. Dreher, S. Schwaiger, W. Schoch, R. Sauer, W. Limmer, A. Brandlmaier, S. T. B. Goennenwein, C. Bihler, and M. S. Brandt, Magnetic anisotropy in (Ga,Mn)As: Influence of epitaxial strain and hole concentration, *Phys. Rev. B* **79**, 195206 (2009).
- [19] H. X. Tang, R. K. Kawakami, D. D. Awschalom, and M. L. Roukes, Giant Planar Hall Effect in Epitaxial (Ga,Mn)As Devices, *Phys. Rev. Lett.* **90**, 107201 (2003).
- [20] L. V. Titova, M. Kutrowski, X. Liu, R. Chakarvorty, W. L. Lim, T. Wojtowicz, J. K. Furdyna, and M. Dobrowolska, Competition between cubic and uniaxial anisotropy in $\text{Ga}_{1-x}\text{Mn}_x\text{As}$ in the low-Mn-concentration limit, *Phys. Rev. B* **72**, 165205 (2005).
- [21] K. Hamaya, T. Watanabe, T. Taniyama, A. Oiwa, Y. Kitamoto, and Y. Yamazaki, Magnetic anisotropy switching in (Ga,Mn)As with increasing hole concentration, *Phys. Rev. B* **74**, 045201 (2006).
- [22] X. Liu and J. K. Furdyna, Ferromagnetic resonance in $\text{Ga}_{1-x}\text{Mn}_x\text{As}$ dilute magnetic semiconductors, *J. Phys. Condens. Matter* **18**, R245 (2006).
- [23] K. Pappert, C. Gould, M. Sawicki, J. Wenisch, K. Brunner, G. Schmidt, and L. W. Molenkamp, Detailed transport investigation of the magnetic anisotropy of (Ga,Mn)As, *New J. Phys.* **9**, 354 (2007).
- [24] L. Thevenard, L. Largeau, O. Mauguin, A. Lemaître, K. Khazen, and H. J. von Bardeleben, Evolution of the magnetic anisotropy with carrier density in hydrogenated $\text{Ga}_{1-x}\text{Mn}_x\text{As}$, *Phys. Rev. B* **75**, 195218 (2007).
- [25] C. Gould, S. Mark, K. Pappert, R. G. Dengel, J. Wenisch, R. P. Campion, A. W. Rushforth, D. Chiba, Z. Li, X. Liu, W. Van Roy, H. Ohno, J. K. Furdyna, B. Gallagher, K. Brunner, G. Schmidt, and L. W. Molenkamp, An extensive comparison of anisotropies in mbe grown (Ga,Mn)As material, *New J. Phys.* **10**, 055007 (2008).
- [26] Y. Nishitani, D. Chiba, M. Endo, M. Sawicki, F. Matsukura, T. Dietl, and H. Ohno, Curie temperature versus hole concentration in field-effect structures of $\text{Ga}_{1-x}\text{Mn}_x\text{As}$, *Phys. Rev. B* **81**, 045208 (2010).
- [27] M. Sawicki, D. Chiba, A. Korbecka, Yu Nishitani, J. A. Majewski, F. Matsukura, T. Dietl, and H. Ohno, Experimental probing of the interplay between ferromagnetism and localization in (Ga,Mn)As, *Nat. Phys.* **6**, 22 (2010).
- [28] O. Proselkov, D. Szentkiel, W. Stefanowicz, M. Aleszkiewicz, J. Sadowski, T. Dietl, and M. Sawicki, Thickness dependent magnetic properties of (Ga,Mn)As ultrathin films, *Appl. Phys. Lett.* **100**, 262405 (2012).
- [29] L. Chen, F. Matsukura, and H. Ohno, Electric-Field Modulation of Damping Constant in a Ferromagnetic Semiconductor (Ga,Mn)As, *Phys. Rev. Lett.* **115**, 057204 (2015).
- [30] T. Dietl, Interplay between carrier localization and magnetism in diluted magnetic and ferromagnetic semiconductors, *J. Phys. Soc. Jpn.* **77**, 031005 (2008).
- [31] A. Richardella, P. Roushan, S. Mack, B. Zhou, D. A. Huse, D. D. Awschalom, and A. Yazdani, Visualizing critical correlations near the metal-insulator transition in $\text{Ga}_{1-x}\text{Mn}_x\text{As}$, *Science* **327**, 665 (2010).
- [32] M. Sawicki, Magnetic properties of (Ga,Mn)As, *J. Mag. Magn. Mater.* **300**, 1 (2006).
- [33] M. Adell, L. Ilver, J. Kanski, V. Stanciu, P. Svedlindh, J. Sadowski, J. Z. Domagala, F. Terki, C. Hernandez, and S. Charar, Postgrowth annealing of (Ga,Mn)As under as capping: An alternative way to increase T_C , *Appl. Phys. Lett.* **86**, 112501 (2005).
- [34] K. W. Edmonds, P. Bogusławski, K. Y. Wang, R. P. Campion, S. N. Novikov, N. R. S. Farley, B. L. Gallagher, C. T. Foxon, M. Sawicki, T. Dietl, M. Buongiorno Nardelli, and J. Bernholc, Mn Interstitial Diffusion in (Ga,Mn)As, *Phys. Rev. Lett.* **92**, 037201 (2004).
- [35] J. Sadowski, R. Mathieu, P. Svedlindh, J. Z. Domagała, J. Bak-Misiuk, K. Swiatek, M. Karlsteen, J. Kanski, L. Ilver, H. Åsklund, and U. Södervall, Structural and magnetic properties of GaMnAs layers with high mn-content grown by migration-enhanced epitaxy on gaas(100) substrates, *Appl. Phys. Lett.* **78**, 3271 (2001).
- [36] K. Gas, J. Z. Domagala, R. Jakiela, G. Kunert, P. Dłuzewski, E. Piskorska-Hommel, W. Paszkowicz, D. Szentkiel, M. J. Winiarski, D. Kowalska, R. Szukiewicz, T. Baraniecki, A. Miszczuk, D. Hommel, and M. Sawicki, Impact of substrate temperature on magnetic properties of plasma-assisted molecular beam epitaxy grown (Ga,Mn)N, *J. Alloys Compd.* **747**, 946 (2018).
- [37] M. Sawicki, W. Stefanowicz, and A. Ney, Sensitive SQUID magnetometry for studying nanomagnetism, *Semicon. Sci. Technol.* **26**, 064006 (2011).
- [38] M. Birowska, C. Śliwa, J. A. Majewski, and T. Dietl, Origin of Bulk Uniaxial Anisotropy in Zinc-Blende Dilute Magnetic Semiconductors, *Phys. Rev. Lett.* **108**, 237203 (2012).
- [39] M. Birowska, C. Śliwa, and J. A. Majewski, Energetic, electronic, and magnetic properties of Mn pairs on reconstructed (001) GaAs surfaces, *Phys. Rev. B* **95**, 115311 (2017).
- [40] M. Sawicki, K.-Y. Wang, K. W. Edmonds, R. P. Campion, C. R. Staddon, N. R. S. Farley, C. T. Foxon, E. Papis, E. Kamińska, A. Piotrowska, T. Dietl, and B. L. Gallagher, In-plane uniaxial anisotropy rotations in (Ga,Mn)As thin films, *Phys. Rev. B* **71**, 121302(R) (2005).
- [41] J. O. Artman, Ferromagnetic resonance in metal single crystals, *Phys. Rev.* **105**, 74 (1957).
- [42] T. Hayashi, Y. Hashimoto, S. Katsumoto, and Y. Iye, Effect of low-temperature annealing on transport and magnetism of diluted magnetic semiconductor (Ga,Mn)As, *Appl. Phys. Lett.* **78**, 1691 (2001).
- [43] K. W. Edmonds, K. Y. Wang, R. P. Campion, A. C. Neumann, N. R. S. Farley, B. L. Gallagher, and C. T. Foxon, High Curie temperature GaMnAs obtained by resistance-monitored annealing, *Appl. Phys. Lett.* **81**, 4991 (2002).
- [44] K. Y. Wang, K. W. Edmonds, R.P. Campion, B. L. Gallagher, N. R. S. Farley, C. T. Foxon, M. Sawicki, P. Bogusławski, and

- T. Dietl, Influence of the Mn interstitials on the magnetic and transport properties of (Ga,Mn)As, *J. Appl. Phys.* **95**, 6512 (2004).
- [45] P. Kossacki, D. Ferrand, A. Arnoult, J. Cibert, S. Tatarenko, A. Wasiela, Y. Merle d'Aubigné, J.-L. Staehli, J.-D. Ganiere, W. Bardyszewski, K. Świątek, M. Sawicki, J. Wróbel, and T. Dietl, Ordered magnetic phase in $\text{Cd}_{1-x}\text{Mn}_x\text{Te}/\text{Cd}_{1-y-z}\text{Mg}_y\text{Zn}_z\text{Te} : \text{N}$ heterostructures: Magneto-optical studies, *Physica E* **6**, 709 (2000).
- [46] C. Bihler, M. Althammer, A. Brandlmaier, S. Geprägs, M. Weiler, M. Opel, W. Schoch, W. Limmer, R. Gross, M. S. Brandt, and S. T. B. Goennenwein, $\text{Ga}_{1-x}\text{Mn}_x\text{As}$ /piezoelectric actuator hybrids: A model system for magnetoelastic magnetization manipulation, *Phys. Rev. B* **78**, 045203 (2008).
- [47] O. M. Fedorych, E. M. Hankiewicz, Z. Wilamowski, and J. Sadowski, Single ion anisotropy of Mn-doped GaAs measured by electron paramagnetic resonance, *Phys. Rev. B* **66**, 045201 (2002).
- [48] Y. Yuan, C. Xu, R. Hübner, R. Jakiela, R. Böttger, M. Helm, M. Sawicki, T. Dietl, and S. Zhou, Interplay between localization and magnetism in (Ga,Mn)As and (In,Mn)As, *Phys. Rev. Materials* **1**, 054401 (2017).
- [49] Y. Yuan, M. Wang, C. Xu, R. Hübner, R. Böttger, R. Jakiela, M. Helm, M. Sawicki, and S. Zhou, Electronic phase separation in insulating (Ga,Mn)As with low compensation: Superparamagnetism and hopping conduction, *J. Phys. Condens. Matter* **30**, 095801 (2018).
- [50] L. Gluba, O. Yastrubchak, J. Z. Domagala, R. Jakiela, T. Andrearczyk, J. Zuk, T. Wosinski, J. Sadowski, and M. Sawicki, Band structure evolution and the origin of magnetism in (Ga,Mn)As: From paramagnetic through superparamagnetic to ferromagnetic phase, *Phys. Rev. B* **97**, 115201 (2018).
- [51] A. Siusys, J. Sadowski, M. Sawicki, S. Kret, T. Wojciechowski, K. Gas, W. Szuszkiewicz, A. Kaminska, and T. Story, All-wurtzite (In,Ga)As-(Ga,Mn)As core-shell nanowires grown by molecular beam epitaxy, *Nano Lett.* **14**, 4263 (2014).
- [52] J. Sadowski, S. Kret, A. Siusys, T. Wojciechowski, K. Gas, M. F. Islam, C. M. Canali, and M. Sawicki, Wurtzite (Ga,Mn)As nanowire shells with ferromagnetic properties, *Nanoscale* **9**, 2129 (2017).
- [53] M. A. Paalanen and R. N. Bhatt, Transport and thermodynamic properties across the metal-insulator transition, *Physica B* **169**, 223 (1991).
- [54] F. Matsukura, M. Sawicki, T. Dietl, D. Chiba, and H. Ohno, Magnetotransport properties of metallic (Ga,Mn)As films with compressive and tensile strain, *Physica E* **21**, 1032 (2004).
- [55] M. Kodzuka, T. Ohkubo, K. Hono, F. Matsukura, and H. Ohno, 3DAP analysis of (Ga,Mn)As diluted magnetic semiconductor thin film, *Ultramicroscopy* **109**, 644 (2009).
- [56] K. W. Edmonds, N. R. S. Farley, T. K. Johal, G. van der Laan, R. P. Campion, B. L. Gallagher, and C. T. Foxon, Ferromagnetic moment and antiferromagnetic coupling in (Ga,Mn)As thin films, *Phys. Rev. B* **71**, 064418 (2005).
- [57] K. Olejník, M. H. S. Owen, V. Novák, J. Mašek, A. C. Irvine, J. Wunderlich, and T. Jungwirth, Enhanced annealing, high Curie temperature and low-voltage gating in (Ga,Mn)As: A surface oxide control study, *Phys. Rev. B* **78**, 054403 (2008).
- [58] D. Hrabovsky, E. Vanelle, A. R. Fert, D. S. Yee, J. P. Redoules, J. Sadowski, J. Kański, and L. Ilver, Magnetization reversal in GaMnAs layers studied by Kerr effect, *Appl. Phys. Lett.* **81**, 2806 (2002).